

f_K/f_π in iso-symmetric QCD and the CKM matrix unitarity

Alessandro Conigli ^{a,b}, Julien Frison ^c, Alejandro Sáez ^d

^a Helmholtz Institute Mainz, Johannes Gutenberg University, Mainz, Germany

^b GSI Helmholtz Centre for Heavy Ion Research, Darmstadt, Germany

^c John von Neumann-Institut für Computing NIC,

Deutsches Elektronen-Synchrotron DESY, Platanenallee 6, 15738 Zeuthen, Germany

^d Instituto de Física Corpuscular (IFIC), CSIC-Universitat de València, 46071, Valencia, Spain

Abstract: We present lattice results for f_K/f_π in the iso-symmetric limit of pure QCD (isoQCD) with $N_f = 2 + 1$ flavours, along with a determination of $|V_{us}|/|V_{ud}|$ and a study on the unitarity of the first row of the Cabibbo-Kobayashi-Maskawa (CKM) matrix after introducing strong isospin-breaking and QED effects. The results obtained are based on a combination of a Wilson unitary action and the mixed-action setup introduced in [1, 2]. The combination of the two regularisations enables a more precise control over the continuum-limit extrapolation.

1 Introduction

In precision era hadronic physics, the ability to make precise predictions of the Standard Model is of the utmost importance for conducting both direct and indirect searches for New Physics. The quark-flavour sector of the Standard Model constitutes a rich arena for this undertaking, where the non-perturbative nature of the strong coupling plays a crucial role. In this context, a first-principles approach to compute hadronic contributions to different physical phenomena, as provided by Lattice QCD, is required. Examples of such processes where non-perturbative input is needed include leptonic and semileptonic meson decays, which provide access to the Cabibbo-Kobayashi-Maskawa (CKM) matrix elements.

The main topic of this work is the computation of f_{K^\pm}/f_{π^\pm} . This quantity allows to extract the ratio of CKM matrix elements $|V_{us}|/|V_{ud}|$ employing the experimental photon inclusive ratio of decay rates

$$\frac{\Gamma(K \rightarrow l\bar{\nu}_l[\gamma])}{\Gamma(\pi \rightarrow l\bar{\nu}_l[\gamma])} = \frac{|V_{us}|^2}{|V_{ud}|^2} \frac{f_{K^\pm}^2}{f_{\pi^\pm}^2} \frac{m_{K^\pm} \left(1 - \frac{m_l^2}{m_{K^\pm}^2}\right)^2}{m_{\pi^\pm} \left(1 - \frac{m_l^2}{m_{\pi^\pm}^2}\right)^2} \times (1 + \delta_{\text{EM}}^K - \delta_{\text{EM}}^\pi), \quad (1.1)$$

where $\delta_{\text{EM}}^{K(\pi)}$ parameterises the QED contributions to $\Gamma(K(\pi) \rightarrow l\bar{\nu}_l[\gamma])$ [3, 4]. Furthermore, one can subsequently obtain a determination of $|V_{us}|$ employing the value of $|V_{ud}|$ as given from super-allowed nuclear β -decays [5], and perform a unitarity test of the first row of the CKM matrix.

In the lattice, the isospin-symmetric limit of pure QCD (isoQCD) is what is most often simulated, with two mass-degenerate light quarks and vanishing electromagnetic coupling $\alpha = 0$. In order to gain access to the ratio f_{K^\pm}/f_{π^\pm} in the full theory, we compute f_K/f_π in isoQCD and later correct for strong isospin-breaking effects. For these effects, as well as for the QED corrections in Eq. (1.1), different approaches exist in the literature [3, 4, 6, 7]. Though in principle it is desirable to have a fully non-perturbative determination of these corrections, we find that the final error of our results is completely dominated by the lattice uncertainty of f_K/f_π in isoQCD, reducing thus the impact of what one uses to correct for strong isospin-breaking and QED effects.

The computation of the ratio f_K/f_π in isoQCD is an unambiguous prediction that can be directly compared to lattice computations by other groups, as long as the input needed to define the physical point is fixed, e.g. as in the Edinburgh Consensus [8].

For our lattice setup, we employ $N_f = 2 + 1$ flavours, i.e. two mass-degenerate light and one strange flavours, based on CLS ensembles [9, 10]. Two different lattice regularisations are employed: the first is a Wilson unitary one [9], with Wilson fermions both in the sea and the valence sectors; the second is a mixed action one [1, 2], employing Wilson fermions in the sea and Wilson twisted mass (Wtm) [11, 12] fermions in the valence. The latter was properly tuned in order to guarantee unitarity in the continuum limit by matching the pion and kaon masses in the sea and valence sectors. This ensures that the physical quark masses in both sectors agree, recovering unitarity in the continuum limit. The combination of both lattice regularisations enables a precise control of the continuum-limit extrapolation and the enhancement of the statistical precision of the final result.

All the ensembles employed have a volume of $m_\pi L \gtrsim 4$ and we correct for finite-volume effects through (finite-volume) next-to-leading order (NLO) Chiral Perturbation Theory (χ PT) for all the observables of interest. We find the correction to be by far subleading at the current statistical precision (cf. Section 3).

In order to define the physical point at which to perform the chiral interpolation of our f_K/f_π lattice data we employ the pion and kaon pseudoscalar masses, expressed in units of the pion decay constant. This is equivalent to setting the scale with f_π . These three quantities are prescribed by the Edinburgh Consensus¹ and FLAG 24 [8] to be

$$m_\pi^{\text{ph}} = 135 \text{ MeV}, \quad m_K^{\text{ph}} = 494.6 \text{ MeV}, \quad f_\pi^{\text{ph}} = 130.5 \text{ MeV}, \quad (1.2)$$

in isoQCD. Using f_π to set the scale, as opposed to employing a theory scale (e.g. gradient flow scales t_0, w_0 [13, 14]), offers the benefit that its physical value is already known, as evidenced by Eq. (1.2), and thus one does not rely on the continuum-limit extrapolation of one of these scales. Conversely, f_π has a strong chiral dependence. However, this effect can be properly addressed in our analysis thanks to the inclusion of physical point ensembles.

This work is structured as follows. In Section 2 we briefly review the basic details of our lattice setup, which is discussed in greater detail in [1, 2]. In Section 3 we introduce our strategy to correct for finite-volume effects in the relevant mesonic observables, based on NLO χ PT. In Section 4 the strategy for interpolating our f_K/f_π lattice data to the physical pion and kaon masses is presented, together with the continuum-limit extrapolation. To this end, we explore different fit

¹<https://indico.ph.ed.ac.uk/event/257/>

functions and cuts in data in order to assess the systematic uncertainty related to the chiral-continuum extrapolation. In Section 5 we introduce strong isospin-breaking effects in the ratio f_K/f_π and review the impact of QED corrections. We rely on χ PT results with a conservative uncertainty to account for these effects, finding them compatible with the most recent ab initio lattice computations. This allows us to extract $|V_{us}|/|V_{ud}|$ and subsequently $|V_{us}|$ by employing a determination of $|V_{ud}|$ from super-allowed β -decays [5], and to perform a test of the unitarity of the first row of the CKM matrix. Finally, we present our conclusions in Section 6. In Appendix A we provide supplementary material on the impact of modifying the definition of the isoQCD values of the input quantities $m_{\pi,K}$ and f_π . We also estimate the derivatives of f_K/f_π in the isoQCD limit with respect to these quantities.

The estimation of statistical uncertainties has been performed using the Γ -method [15] implementation in the `ADerrors` package [16].

2 Setup

In this section we review the basic features of our setup, with an emphasis on the aspects that are most relevant to the present work. We refer the reader to [1, 2] for a fully detailed discussion of our approach.

The set of lattice ensembles under study were generated by the Coordinated Lattice Simulations (CLS) initiative [10, 17]. They use the Lüscher-Weisz gauge action [18] and non-perturbatively $O(a)$ -improved $N_f = 2 + 1$ Wilson fermions in the sea sector. Open boundary conditions (OBC) are employed in the time direction for the gauge degrees of freedom for most ensembles, in order to avoid topology freezing as the continuum limit is approached.

The ensembles that we include in the analysis follow a chiral trajectory defined by an approximately constant trace of the bare quark mass matrix, imposed by the condition

$$8t_0 \left(m_K^2 + \frac{1}{2} m_\pi^2 \right) \approx \text{const.} \Rightarrow \text{tr}(M_q) = 2m_l + m_s \approx \text{const.} \quad (2.1)$$

More details on the ensembles are provided in Table 1.

For our kinematic variables, we define

$$\rho_2 = \frac{m_\pi^2}{f_\pi^2}, \quad (2.2)$$

$$\rho_4 = \frac{m_K^2 + \frac{1}{2} m_\pi^2}{f_\pi^2}. \quad (2.3)$$

With the input in Eq. (1.2), the physical values ρ_2^{ph} , ρ_4^{ph} are unambiguously determined, thereby defining the physical point at which to chirally-interpolate the f_K/f_π data. Note that we interpolate both in ρ_2 and ρ_4 . We have one ensemble (E250) lying at the physical pion mass. In Fig. 1 we show the range of values explored for these quantities along the ensembles considered in this work.

In the valence sector, the regularisation employed for the Dirac operator is either identical to that utilised in the sea sector (Wilson unitary setup), or a Wilson twisted mass [11, 12] one (mixed-action setup). In the latter case, the valence parameters were tuned in order to match the pion and kaon masses – in units of the lattice spacing – in the sea and valence sectors [1, 2]. This ensures that physical quark masses coincide in both sectors, thereby recovering unitarity of the theory in

the continuum limit, as was checked in [1] through universality tests. Furthermore, the valence sector was tuned to maximal twist by setting the valence light PCAC standard quark mass to zero. This results in automatic $O(a)$ -improvement up to residual sea cutoff effects of $O(ag_0^4 \text{tr} M_q^{\text{sea}})$. For a more thorough exposition about the tuning of the mixed action, see [1, 2].

The two lattice regularisations must share the same continuum limit; however they can exhibit different cutoff effects. Consequently, the analysis of both sets of data in conjunction with the imposition of a common continuum limit can facilitate the control of the extrapolation to vanishing lattice spacing.

The relevant lattice observables for this study are the pseudoscalar masses m_{PS} , employed to define the physical point, and decay constants f_{PS} , with $\text{PS} = \pi, K$. Both set of observables can be extracted from two-point functions involving the pseudoscalar density and axial current. They exhibit clear plateaus, which we extract by model averaging different plateau ranges as proposed in [19]. For more details on this latter subject, we refer to [1, 2].

In Table 2 we present measurements for f_K/f_π , ρ_2 , ρ_4 , while in Table 3 the values of af_π at the SU(3) symmetric point, defined by $m_\pi = m_K \approx 420$ MeV, are shown. The latter will be used as probes for cutoff effects (cf. Section 4). In both tables finite-volume effects are already taken into account (cf. Section 3).

All physical observables are free of $O(a)$ cutoff effects, either thanks to the automatic $O(a)$ -improvement feature of our mixed action, or to the inclusion of the relevant improvement coefficients for the Wilson unitary setup. Once again we refer to [1, 2] for details on improvement, as well as for the relevant renormalisation factors for the decay constants.

3 Finite volume effects

The masses and decay constants of the pion and kaon suffer from finite volume effects, which will be addressed in this section. Finite-volume χ PT enables to correct these effects in our quantities of interest. To NLO and for $X = m_{\pi, K}$, $f_{\pi, K}$, denoting by $X^{(\infty)}$ the infinite volume quantity and by $X^{(L)}$ the finite volume one [25, 26],

$$\begin{aligned} X^{(\infty)} &= X^{(L)} \frac{1}{1 + R_X}, \\ R_{m_\pi} &= \frac{1}{4} \xi_\pi \tilde{g}_1(\lambda_\pi) - \frac{1}{12} \xi_\eta \tilde{g}_1(\lambda_\eta), \quad R_{m_K} = \frac{1}{6} \xi_\eta \tilde{g}_1(\lambda_\eta), \\ R_{f_\pi} &= -\frac{3}{8} \xi_\pi \tilde{g}_1(\lambda_\pi) - \frac{3}{4} \xi_K \tilde{g}_1(\lambda_K) - \frac{3}{8} \xi_\eta \tilde{g}_1(\lambda_\eta), \quad R_{f_K} = -\xi_\pi \tilde{g}_1(\lambda_\pi) - \frac{1}{2} \xi_K \tilde{g}_1(\lambda_K), \\ \xi_{PS} &= \frac{m_{PS}^2}{(4\pi f_\pi)^2}, \quad \lambda_{PS} = m_{PS} L, \quad \tilde{g}_1(x) = \sum_{n=1}^{\infty} \frac{4m(n)}{\sqrt{nx}} K_1(\sqrt{nx}), \end{aligned} \quad (3.1)$$

where $m_\eta^2 = \frac{4}{3} m_K^2 - \frac{1}{3} m_\pi^2$, $K_1(x)$ is the Bessel function of the second kind, and $m(n)$ is given in [25, 26].

The shifts in the values of $m_{\pi, K}$ and $f_{\pi, K}$ due to these contributions are well within one standard deviation, even for the smallest volume considered, corresponding to $m_\pi L = 3.9$ in the H105 ensemble, as can be seen in Fig. 2.

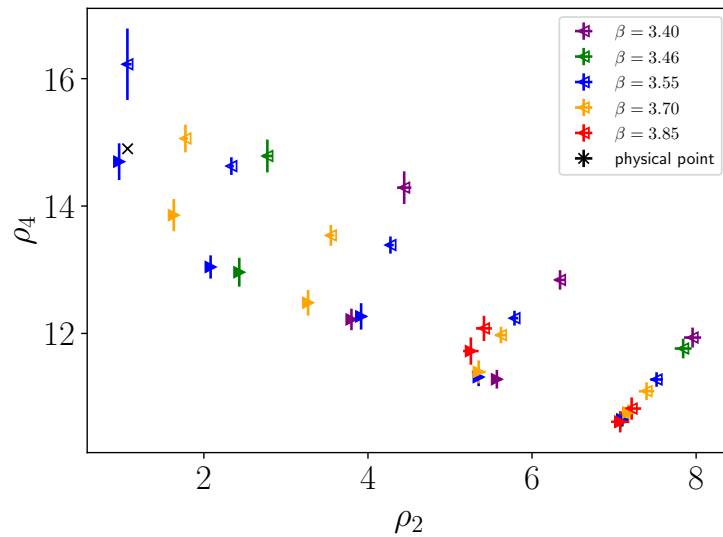


Figure 1: Measured values of ρ_2 , ρ_4 , defined in Eq. (2.2) and Eq. (2.3), for the set of CLS ensembles employed in this work, following the $\text{tr}(M_q) = 2m_l + m_s \approx \text{const.}$ chiral trajectory. Empty points correspond to the Wilson unitary setup, while filled ones correspond to the Wtm mixed action. The difference in ρ_2 and ρ_4 between the Wilson and Wtm mixed action for any given ensemble is due to different cutoff effects in f_π for each regularisation, as the pion and kaon masses – in lattice units – are matched to be the same in both. The physical point, marked by a black cross, is reached by interpolating both in ρ_2 and ρ_4 .

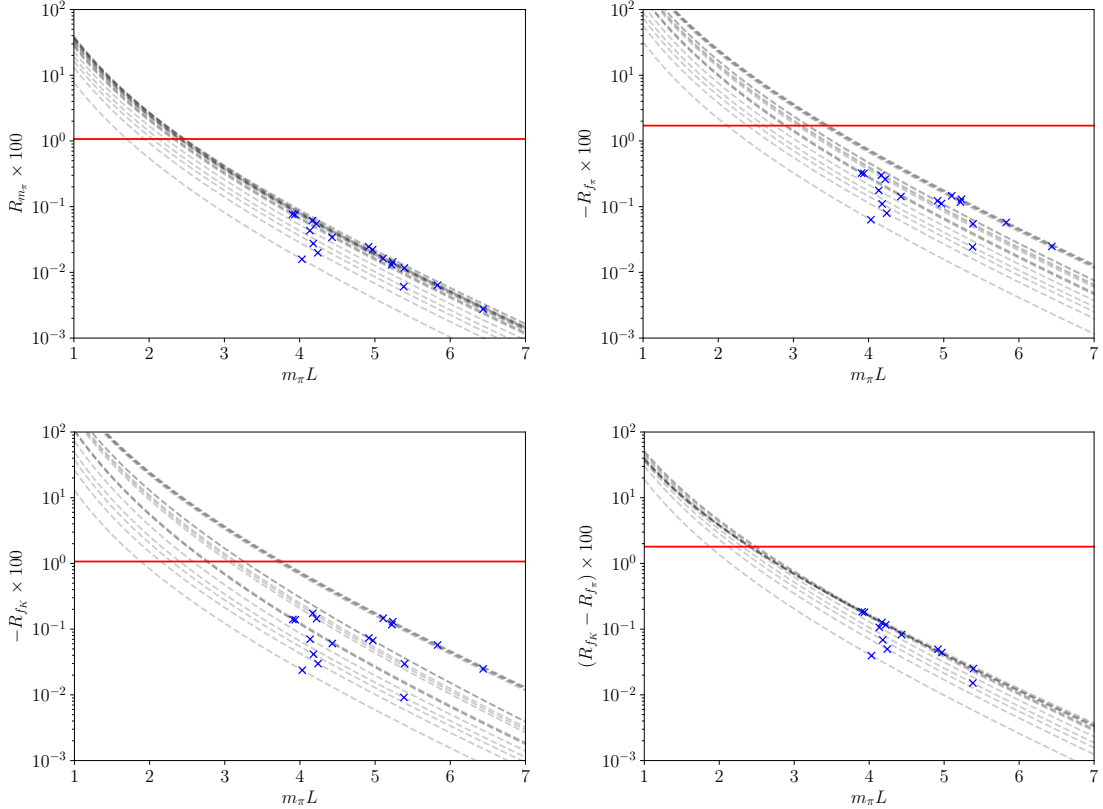


Figure 2: R_X for $X = m_\pi, f_\pi, f_K$ for the set of ensembles considered in this work in the Wilson unitary setup, as given by Eq. (3.1) (blue crosses), together with the expected dependence on $m_\pi L$ for each of these ensembles (grey dashed lines). It can be seen that the finite-volume correction is of a few per mille at most, well below the statistical precision of the lattice data (the red horizontal line shows a representative example of the relative statistical precision). $R_{f_K} - R_{f_\pi}$ in the bottom right plot is the relevant correction factor for the ratio f_K/f_π .

β	a [fm]	id	L/a	T/a	m_π [MeV]	m_K [MeV]	$m_\pi L$	LMD	MDU	N_{cfg}
3.40	0.085	H101r000	32	96	426	426	5.8	no	4004	1001
		H101r001	32	96	426	425	5.8	no	4036	1009
		H102r001	32	96	360	446	4.9	yes	3988	997
		H102r002	32	96	360	446	4.9	yes	4032	1008
		H105r001	32	96	286	470	3.9	yes	3788	947
		H105r002	32	96	286	470	3.9	yes	4168	1042
		H105r005	32	96	286	470	3.9	no	3348	837
3.46	0.075	H400r001	32	96	429	429	5.2	no	2020	505
		H400r002	32	96	429	429	5.2	no	2160	540
		D450r011	64	128	221	483	5.4	yes	4000	250
3.55	0.063	N202r001	48	128	418	418	6.5	no	3596	899
		N203r000	48	128	350	448	5.4	yes	3024	756
		N203r001	48	128	350	448	5.4	yes	3148	787
		N200r000	48	128	288	470	4.4	yes	3424	856
		N200r001	48	128	288	470	4.4	yes	3424	856
		D200r000	64	128	204	488	4.2	yes	8004	2001
		E250r001	96	192	131	497	4.0	yes	4000	100
3.70	0.049	N300r002	48	128	427	427	5.1	no	6084	1521
		N302r001	48	128	350	457	4.2	no	8804	2201
		J303r003	64	192	261	481	4.1	yes	8584	1073
		E300r001	96	192	177	499	4.2	no	4540	227
3.85	0.038	J500r004	64	192	418	418	5.2	no	6288	198
		J500r005	64	192	418	418	5.2	no	5232	130
		J500r006	64	192	418	418	5.2	no	3096	94
		J501r001	64	192	339	453	4.3	no	6536	371
		J501r002	64	192	339	453	4.3	no	4560	248
		J501r003	64	192	339	453	4.3	no	4296	168

Table 1: Set of $N_f = 2 + 1$ CLS ensembles employed in this work. The table includes the values of the bare coupling $\beta = 6/g_0^2$; the spatial and temporal extents of the lattice, as well as approximate values of the lattice spacing a as determined in [1]; the masses of the pion m_π and the kaon m_K ; and $m_\pi L$. Additionally, the number of configurations N_{cfg} and the corresponding length of the Monte Carlo chain in Molecular Dynamics Units (MDU) employed in the computation of the mesonic correlation functions are provided. In all ensembles, open boundary conditions in the time direction are employed for the gauge fields, with the exception of ensembles E250 and D450, which have anti-periodic boundary conditions in time. The column “LMD” refers to whether the reweighting factors were computed following [18] (“yes”) or [20–24] (“no”). We separate by horizontal lines different ensembles and/or false replicas.

ID	ρ_2 [W]	ρ_2 [Wtm]	ρ_4 [W]	ρ_4 [Wtm]	f_K/f_π [W]	f_K/f_π [Wtm]
H101	8.316(76)	7.235(52)	12.47(11)	10.85(8)	1.0	1.0
H102	6.542(56)	5.716(45)	13.35(11)	11.66(8)	1.0509(21)	1.0569(16)
H105	4.617(83)	3.873(49)	14.92(23)	12.51(10)	1.1182(78)	1.1021(33)
H400	8.474(89)	7.524(77)	12.71(13)	11.29(12)	1.0	1.0
D450	2.859(56)	2.503(32)	15.10(22)	13.22(18)	1.1418(66)	1.1422(33)
N202	7.834(60)	7.238(68)	11.75(9)	10.86(10)	1.0	1.0
N203	5.884(38)	5.357(47)	12.61(7)	11.48(10)	1.0540(15)	1.0519(17)
N200	4.351(40)	4.057(36)	13.76(9)	12.83(10)	1.0998(27)	1.1070(34)
D200	2.392(26)	2.142(27)	14.94(11)	13.37(12)	1.1551(33)	1.1343(46)
E250	1.100(43)	0.997(18)	16.41(56)	14.88(26)	1.1952(215)	1.1937(83)
N300	7.965(53)	7.635(60)	11.95(8)	11.45(9)	1.0	1.0
N302	5.668(84)	5.427(72)	12.53(16)	12.00(15)	1.0574(20)	1.0608(42)
J303	3.545(35)	3.326(46)	13.97(12)	13.11(16)	1.1188(44)	1.1161(64)
E300	1.889(38)	1.775(29)	15.79(27)	14.83(18)	1.1735(138)	1.1893(201)
J500	7.443(130)	7.239(165)	11.16(20)	10.86(25)	1.0	1.0
J501	5.374(88)	5.292(118)	12.30(19)	12.12(26)	1.0607(28)	1.0647(51)

Table 2: Measurements of ρ_2 , ρ_4 and f_K/f_π for both the Wilson unitary [W] and Wtm mixed-action [Wtm] setups. The mixed action was tuned in order to impose identical pion and kaon masses in the sea and valence sectors in units of the lattice spacing. The difference between ρ_2 , ρ_4 in the Wilson unitary and mixed-action regularisations therefore comes exclusively from different cutoff effects in f_π for each regularisation. Finally, the ratio f_K/f_π is 1.0 without error in the SU(3) symmetric point by construction. All measurements are corrected for finite-volume effects as detailed in Section 3. Measurements corresponding to false replicas are averaged together. All quantities are renormalised and non-perturbatively $O(a)$ -improved, for a general discussion we refer to [1, 2].

β	af_π^{sym} [W]	af_π^{sym} [Wtm]
3.40	0.06319(28)	0.06774(24)
3.46	0.05620(25)	0.05965(30)
3.55	0.04792(17)	0.04985(19)
3.70	0.03770(11)	0.03850(13)
3.85	0.02991(23)	0.03033(33)

Table 3: Values for af_π at the SU(3) symmetric point, defined by $m_\pi = m_K \approx 420$ MeV, for each β considered in this work, to be employed as probes for the cutoff effects (cf. Section 4). We quote values for both the Wilson unitary [W] and Wtm mixed-action [Wtm] setups, the difference between them being a cutoff effect. Finite-volume effects are included as detailed in Section 3. Results are renormalised and non-perturbatively $O(a)$ -improved, for a general discussion we refer to [1, 2]

4 Chiral-continuum extrapolation

In order to compute the ratio f_K/f_π in isoQCD at the physical point, we need to chirally-interpolate our lattice data to ρ_2^{ph} , ρ_4^{ph} as given in Eq. (1.2), and perform the continuum limit to $a \rightarrow 0$. For the former, we can use χ PT-inspired formulae, as well as Taylor expansions in the pion and kaon masses.

From SU(3) NLO χ PT we have

$$f_\pi = f \left[1 + \frac{16B_0L_5(\mu)}{f^2} m_l + \frac{16B_0L_4(\mu)}{f^2} (2m_l + m_s) - 2\mathcal{L}(m_\pi^2, \mu) - \mathcal{L}(m_K^2, \mu) \right], \quad (4.1)$$

$$\begin{aligned} f_K = f \left[1 + \frac{8B_0L_5(\mu)}{f^2} (m_l + m_s) + \frac{16B_0L_4(\mu)}{f^2} (2m_l + m_s) \right. \\ \left. - \frac{3}{4}\mathcal{L}(m_\pi^2, \mu) - \frac{3}{2}\mathcal{L}(m_K^2, \mu) - \frac{3}{4}\mathcal{L}(m_\eta^2, \mu) \right], \end{aligned} \quad (4.2)$$

where

$$m_\pi^2 = 2B_0 m_l, \quad m_K^2 = B_0(m_l + m_s), \quad m_\eta^2 = \frac{4}{3}m_K^2 - \frac{1}{3}m_\pi^2, \quad (4.3)$$

$$\mathcal{L}(x, \mu) = \frac{x}{(4\pi f)^2} \log \frac{x}{\mu^2}, \quad (4.4)$$

with f the decay constant in the chiral limit, and μ a renormalisation scale. The dependence of the LECs $L_4(\mu)$, $L_5(\mu)$ in μ cancels with that of the chiral logarithms $\mathcal{L}(x, \mu)$, so that physical quantities are μ -independent.

Computing the ratio of decay constants gives

$$\frac{f_K}{f_\pi} = \frac{1 + 8L_5(\mu)q^2 (\rho_4 - \frac{1}{2}\rho_2) - \frac{3}{4}\mathcal{L}_\pi(\mu) - \frac{3}{2}\mathcal{L}_K(\mu) - \frac{3}{4}\mathcal{L}_\eta(\mu)}{1 + 8L_5(\mu)q^2\rho_2 - 2\mathcal{L}_\pi(\mu) - \mathcal{L}_K(\mu)}, \quad (4.5)$$

where

$$q \equiv \frac{f_\pi}{f}, \quad (4.6)$$

$$\mathcal{L}_\pi(\mu) = \frac{\rho_2}{(4\pi)^2} q^2 \log \left(\frac{m_\pi^2}{\mu^2} \right), \quad (4.7)$$

$$\mathcal{L}_K(\mu) = \frac{\rho_4 - \frac{1}{2}\rho_2}{(4\pi)^2} q^2 \log \left(\frac{m_K^2}{\mu^2} \right), \quad (4.8)$$

$$\mathcal{L}_\eta(\mu) = \frac{\frac{4}{3}\rho_4 - \rho_2}{(4\pi)^2} q^2 \log \left(\frac{m_\eta^2}{\mu^2} \right). \quad (4.9)$$

We choose $\mu \equiv f_{\pi K} = \frac{2}{3}(f_K + \frac{1}{2}f_\pi)$ in the spirit of keeping it a constant renormalisation scale, since $f_{\pi K}$ has a weak chiral dependence along our $\text{tr}(M_q) \approx \text{const.}$ trajectory [17]. Furthermore, we treat the $q = f_\pi/f$ factor as a fit parameter, together with the LEC L_5 . This amounts to ignoring the chiral dependence of q due to that of f_π , since it enters as a higher order effect. We observe no discrepancy with this assumption when performing the chiral fits.

To the expression in Eq. (4.5) we need to add cutoff effects, which can be effectively done by expanding the LECs f, L_5 as

$$\begin{aligned} L_5 &\rightarrow L_5 \left(1 + \mathcal{O} \left(a^2 \alpha_S^{\Gamma_i} \right) \right), \\ f &\rightarrow f \left(1 + \mathcal{O} \left(a^2 \alpha_S^{\Gamma_i} \right) \right), \end{aligned} \quad (4.10)$$

with Γ_i the various anomalous dimensions provided for our actions in [27], together with the case $\Gamma_i = 0$. This choice for the form of cutoff effects ensures that f_K/f_π is exactly 1 at the SU(3) symmetric limit, even at finite lattice spacing. As probe for cutoff effects, in the spirit of not relying on any theory scale for the analysis, we will employ $af_\pi^{\text{sym}}(\beta)$ (cf. Table 3), the pion decay constant (in lattice units) at the SU(3) symmetric point for each value of the inverse coupling β . In practice, we substitute

$$\begin{aligned} L_5 q^2 &\rightarrow L_5 q^2 \left(1 + C_1 (af_\pi^{\text{sym}})^2 \alpha_S^{\Gamma_i} \right), \\ q^2 &\rightarrow q^2 \left(1 + C_2 (af_\pi^{\text{sym}})^2 \alpha_S^{\Gamma_i} \right), \end{aligned} \quad (4.11)$$

in Eq. (4.5), with $C_{1,2}$ additional fit parameters.

In order to explore systematic effects in the chiral-continuum extrapolation, it is necessary to test different fit functions and cuts in the data, which we eventually average together. To this end, the first possible variation involves exploring the different available values of Γ_i . However, we observe no sensitivity in the data to this variation,² and thus choose to perform the final analysis only with $\Gamma_i = 0$ in order not to explore redundant models. We note that the smallest possible value of Γ_i for both our actions is $\Gamma_i = -0.11$.

The ratio in Eq. (4.5) can also be expanded to give a new model

$$\frac{f_K}{f_\pi} = 1 - 12L_5(\mu)q^2\rho_2 + 8L_5(\mu)q^2\rho_4 + \frac{5}{4}\mathcal{L}_\pi(\mu) - \frac{1}{2}\mathcal{L}_K(\mu) - \frac{3}{4}\mathcal{L}_\eta(\mu), \quad (4.12)$$

where again we use Eq. (4.11) in order to add cutoff effects.

Another possibility for model exploration is to use $\mu = f_\pi$ in the definition of the chiral logarithms in Eqs. (4.7)–(4.9) and the LEC L_5 . Again, this assumes that the chiral dependence introduced in μ can be neglected as a higher order effect.

We can also use a Taylor expansion in ρ_2 and ρ_4 . In order to constrain that the expansion goes to 1 in the SU(3) symmetric limit, we expand the chiral logarithms $\mathcal{L}_\pi, \mathcal{L}_K, \mathcal{L}_\eta$ around the symmetric point in Eq. (4.12), arriving at

$$\frac{f_K}{f_\pi} = 1 + A(2\rho_4 - 3\rho_2) + B \left(\frac{3}{8}\rho_2^2 - \frac{11}{6}\rho_4^2 + \frac{5}{2}\rho_2\rho_4 \right). \quad (4.13)$$

We find that expanding both A, B in an analogous way to Eq. (4.10) always results in the fit parameter controlling the cutoff effects in B being compatible with zero and thus in inflated errors,³

²The central value of f_K/f_π in the continuum changes only a 0.4% of σ when varying from $\Gamma_{\min} = -0.11$ to $\Gamma_{\max} = 0.76$, corresponding to the minimum possible and maximum known values of Γ_i for both our Wilson unitary and Wtm mixed-action setups [27].

³Furthermore, when employing an information criterion-based model average, e.g. employing the Takeuchi Information Criterion [28] or the Akaike Information Criterion [19], this model always results in zero weight because of this behaviour.

so we only consider

$$\frac{f_K}{f_\pi} = 1 + \left(A + C (a f_\pi^{\text{sym}})^2 \alpha_S^{\Gamma_i} \right) \times (2\rho_4 - 3\rho_2) + B \left(\frac{3}{8} \rho_2^2 - \frac{11}{6} \rho_4^2 + \frac{5}{2} \rho_2 \rho_4 \right), \quad (4.14)$$

Finally, we also test a Taylor fit without any constraint in the SU(3) symmetric limit. In this case we find that the fit is only sensitive to the following terms

$$\frac{f_K}{f_\pi} = A_0 + A_1 \rho_2 + A_2 \rho_2^2 + B_1 \rho_4 + C (a f_\pi^{\text{sym}})^2 \alpha_S^{\Gamma_i}. \quad (4.15)$$

Adding any other term results in coefficients compatible with zero and a continuum limit compatible with that of the model in Eq. (4.15) with inflated errors (cf. footnote 3).

Finally, in addition to the different fit function variations given above, we also explore performing cuts in the data. In particular, we test removing the coarsest lattice spacing $\beta = 3.40$, the heaviest pions $m_\pi < 360$ MeV,⁴ and removing volumes with $m_\pi L < 4.2$.

In Fig. 5 we show the chiral-continuum extrapolation for two representative models, with different fit functions and cuts in the data.

In order to quantify the quality of fits we employ the p-value [29]. After selecting all models with p-value > 0.1 , we employ the following scheme to compute a model average result:⁵ (i) compute a model average central value and statistical uncertainty with a weighted average of all models, weighting with the errors; (ii) compute a total model average uncertainty (systematic and statistical) by taking half the maximum spread between models; and (iii) considering that systematic and statistical uncertainties add up in quadrature to give the total model average uncertainty, extract the corresponding systematic uncertainty from (i) and (ii). The result is

$$\frac{f_K}{f_\pi} = 1.1872(59)_{\text{stat}}(84)_{\chi-\text{cont}}, \quad (4.16)$$

where “ $\chi - \text{cont}$ ” labels the systematic uncertainty of the model average. The model average is presented in Fig. 3. We observe the maximum spread between models to be associated with models that employ $\mu = f_\pi$ or $\mu = f_{\pi K}$ in Eqs. (4.7)–(4.9); the use of Eq. (4.12) or Eq. (4.5); and cuts in the pion masses. We interpret this fact as signaling that higher order effects in the chiral dependence of f_K/f_π are the main source of systematic uncertainty in Eq. (4.16), and thus the need in the future to include NNLO terms in Eqs. (4.1) and (4.2). We stress that with our current data set we are not able to resolve these terms.

Finally, in Fig. 4 we show the contribution of the different lattice ensembles to the statistical error in Eq. (4.16).

5 CKM matrix unitarity

In order to test the unitarity of the first row of the CKM matrix

$$|V_{ud}|^2 + |V_{us}|^2 + |V_{ub}|^2 \stackrel{?}{=} 1, \quad (5.1)$$

⁴Note that the symmetric point, corresponding to $m_\pi \approx 420$ MeV, having by construction $f_K/f_\pi = 1$ with no error, does not contribute to the χ^2 .

⁵No significant change in the final result is seen by performing a model average based on the Takeuchi Information Criterion [28] or the Akaike Information Criterion [19].

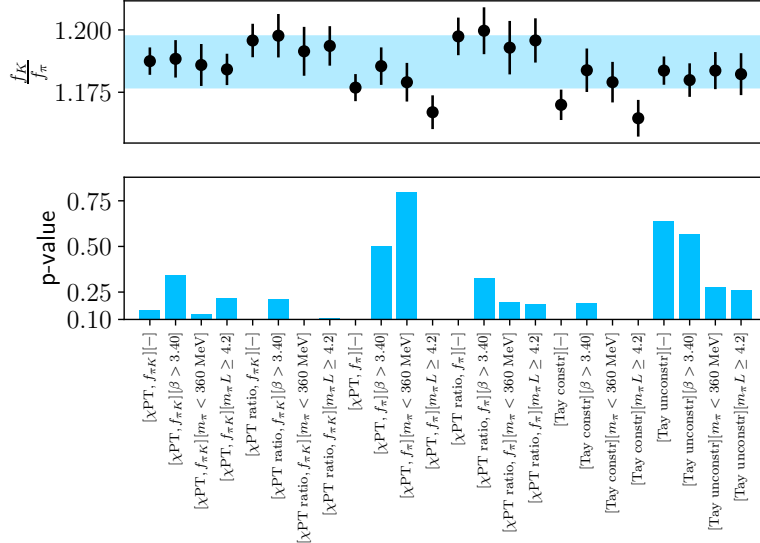


Figure 3: Model exploration for the chiral-continuum extrapolation of the ratio f_K/f_π . In the first bracket, labels $[\chi\text{PT}]$ and $[\chi\text{PT ratio}]$ refer to the use of Eq. (4.12) and Eq. (4.5) respectively, with cutoff effects added according to Eq. (4.11), while $f_{\pi K}$ or f_π refers to what was used for the scale μ inside the chiral logarithms in Eqs. (4.7)–(4.9). $[\text{Tay constr}]$ refers to Eq. (4.14), and $[\text{Tay unconstr}]$ to Eq. (4.15). The second label indicates which data are included: $[-]$ means all data are used, $[\beta > 3.40]$ that the coarsest lattice spacing is removed, $[m_\pi < 360 \text{ MeV}]$ that only ensembles with pion masses smaller than 360 MeV are included in the analysis, and $[m_\pi L \geq 4.2]$ the same for lattices with the volume satisfying this condition. The horizontal band in the top panel represents the final quoted result in Eq. (4.16), with statistical and systematic uncertainties added in quadrature.

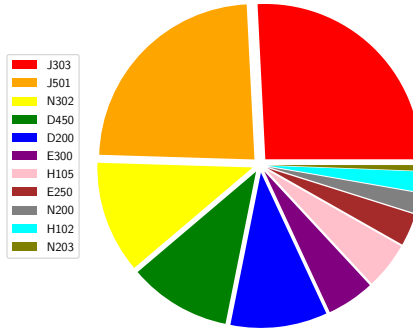


Figure 4: Contribution of the different lattice ensembles to the statistical error squared in Eq. (4.16).

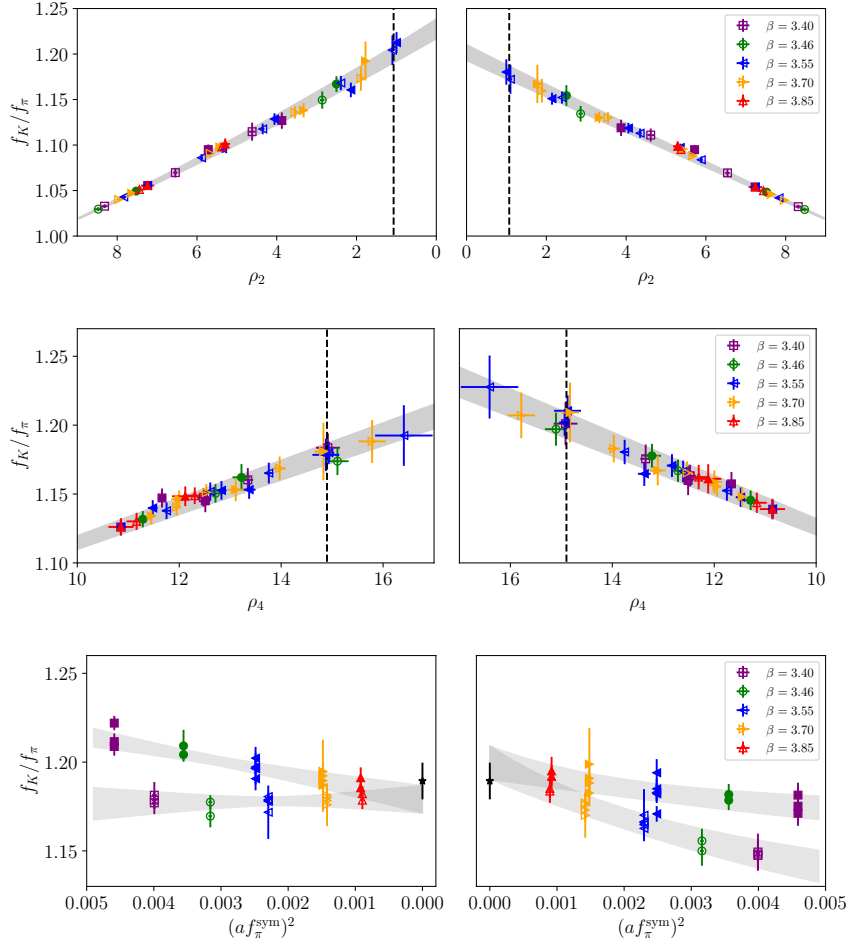


Figure 5: *Left column:* chiral-continuum extrapolation employing Eq. (4.12), using $\mu = f_\pi$ in the definition of the chiral logarithms, and adding cutoff effects according to Eq. (4.11) with $\Gamma_i = 0$, removing $m_\pi > 360$ MeV. *Right column:* chiral-continuum extrapolation employing Eq. (4.5), using $\mu = f_\pi$, and adding cutoff effects according to Eq. (4.11) with $\Gamma_i = 0$, removing the coarsest lattice spacing $\beta = 3.40$. In the two top plots, the points in the y -axis are projected to ρ_4^{ph} and vanishing lattice spacing, while in the two middle plots they are projected to ρ_2^{ph} and vanishing lattice spacing. The vertical dashed line marks the position of the physical point, and the bands correspond to the mass-dependence in the continuum. Finally, in the two bottom plots the data in the y -axis are projected to both ρ_2^{ph} , ρ_4^{ph} . The two bands in each plot correspond to the cutoff dependence for both the Wilson unitary and Wtm mixed-actions setups. Empty points are computed with the Wilson unitary action, while filled ones are with the mixed action. The two models shown correspond to the ones giving the lowest and highest results that enter in the model average (cf. Fig. 3), and thus define the width of our error band in Eq. (4.16), corresponding to the black star point in the two bottom plots.

it is necessary to have access to these three matrix elements. To this end, $|V_{ud}|$ can be extracted with high precision from super-allowed nuclear β -decays, while $|V_{ub}|$ can be neglected given its small value and the current precision for the other two matrix elements [5]. Lastly, we extract $|V_{us}|/|V_{ud}|$ through the use of Eq. (1.1), a lattice determination of f_{K^\pm}/f_{π^\pm} – after including strong isospin-breaking effects in Eq. (4.16) – and taking into account the QED correction factor $(1 + \delta_{\text{EM}}^K - \delta_{\text{EM}}^\pi)$. This allows us to extract $|V_{us}|$ by using the aforementioned value of $|V_{ud}|$.

In order to include strong isospin-breaking effects in our determination of f_K/f_π given in Eq. (4.16), to NLO in $\text{SU}(3)$ χ PT [8, 30]

$$\frac{f_{K^\pm}^2}{f_{\pi^\pm}^2} = \frac{f_K^2}{f_\pi^2} \times (1 + \delta_{\text{SU}(2)}), \quad (5.2)$$

$$\delta_{\text{SU}(2)} = \sqrt{3}\epsilon_{\text{SU}(2)} \left[-\frac{4}{3}(f_K/f_\pi - 1) + \frac{2}{3(4\pi)^2 f^2} \left(m_K^2 - m_\pi^2 - m_\pi^2 \log \frac{m_K^2}{m_\pi^2} \right) \right], \quad (5.3)$$

$$\epsilon_{\text{SU}(2)} = \sqrt{3}/4R, \quad R \equiv \frac{m_s - m_{ud}}{m_d - m_u}. \quad (5.4)$$

To compute $\delta_{\text{SU}(2)}$, we use $f = 113(28)$ MeV, $R = 38.1(1.5)$ as reported by [8], resulting in

$$\delta_{\text{SU}(2)} = -0.0038(7). \quad (5.5)$$

However, given the unknown size of higher order corrections, we opt to take a conservative approach and assign a 100% uncertainty to $\delta_{\text{SU}(2)}$, resulting in

$$\delta_{\text{SU}(2)} = -0.004(4). \quad (5.6)$$

With this result, we obtain for the ratio of decay constants, including strong isospin-breaking corrections

$$\frac{f_{K^\pm}}{f_{\pi^\pm}} = 1.1848(59)_{\text{stat}}(84)_{\chi-\text{cont}}(24)_{\text{SU}(2)}, \quad (5.7)$$

where “stat” and “ $\chi - \text{cont}$ ” correspond to the errors in Eq. (4.16), i.e. they are uncertainties related to the lattice data, and “ $\text{SU}(2)$ ” corresponds to the uncertainty in Eq. (5.6). In Fig. 6 we compare our final estimate with results from other collaborations that enter the FLAG average for $N_f = 2 + 1$ [8].

For the QED correction $\delta_{\text{EM}}^{\text{PS}}$ to the experimental measurement of $\Gamma(\text{PS} \rightarrow l\bar{\nu}_l[\gamma])$, $\text{PS} = \pi, K$, we reproduce the same steps as in [3, 30], and we will argue for a conservative choice of the corresponding uncertainty. The $\delta_{\text{EM}}^{\text{PS}}$ factor reads

$$\begin{aligned} \delta_{\text{EM}}^{\text{PS}} = & -\frac{\alpha}{\pi} \left[-F \left(\frac{m_l}{m_{\text{PS}}} \right) + \frac{3}{2} \log \left(\frac{m_\rho}{m_{\text{PS}}} \right) + c_1^{\text{PS}} \right. \\ & \left. + \frac{m_l^2}{m_\rho^2} \left(2c_2^{\text{PS}} \log \left(\frac{m_\rho}{m_l} \right) + c_3^{\text{PS}} + c_4^{\text{PS}} \frac{m_l}{m_{\text{PS}}} \right) - 2\tilde{c}_2^{\text{PS}} \frac{m_{\text{PS}}^2}{m_\rho^2} \log \left(\frac{m_\rho}{m_l} \right) + \text{h.o.} \right], \end{aligned} \quad (5.8)$$

where the first term is the universal long distance contribution to one-loop, assuming that the pseudoscalar state PS is point-like, while the terms proportional to c_i^{PS} , \tilde{c}_i^{PS} parameterise the structure-dependent part. To the current precision it is enough to consider the c_1^{PS} terms,⁶ whose

⁶Adding the missing terms, using the results in [30, 38], amounts to a shift of a 16% of σ in the central value w.r.t. Eq. (5.11).

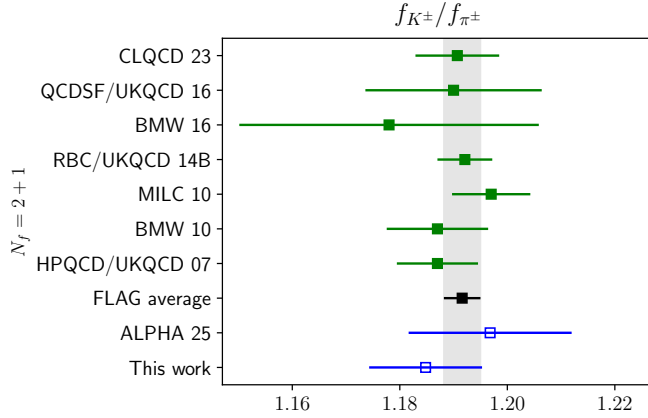


Figure 6: Comparison of our result for f_{K^\pm}/f_{π^\pm} with strong isospin-breaking corrections, as given in Eq. (5.7), to other group's results entering the FLAG average for $N_f = 2 + 1$ [8]. CLQCD 23 refers to [31], QCDSF/UKQCD 16 to [32], BMW 16 to [33], RBC/UKQCD 14B to [34], MILC 10 to [35], BMW 10 to [36] and HPQCD/UKQCD 07 to [37]. The point ALPHA 25 corresponds to our previous determination of f_K in [1] based on an analysis setting the scale employing the intermediate scale $\sqrt{t_0}$.

values are given, using large- N_c methods, by [4, 38, 39]

$$c_1^\pi = -2.5(5), \quad c_1^K = -1.9(5). \quad (5.9)$$

Since we are only interested in the combination $(1 + \delta_{\text{EM}}^K - \delta_{\text{EM}}^\pi)$ as evident in Eq. (1.1), the relevant quantity to us is

$$\Delta c_1 \equiv c_1^K - c_1^\pi = 0.6(6), \quad (5.10)$$

where we took only the central values in Eq. (5.9) and then assumed 100% uncertainty for Δc_1 , in order to cover the structureless pion and kaon limit in which $\Delta c_1 = 0$, which we consider to be the most conservative choice. Taking $l = \mu$ and with the function $F(x)$ explicitly given in [3], we get

$$\delta_{\text{EM}}^K - \delta_{\text{EM}}^\pi = -0.0072(14). \quad (5.11)$$

With the results in Eq. (5.6) and Eq. (5.11), as an intermediate comparison with recent lattice computations we quote the joint quantity $\delta R_{K\pi} = \delta_{\text{SU}(2)} + \delta_{\text{EM}}^K - \delta_{\text{EM}}^\pi$, for which we obtain

$$\delta R_{K\pi} = -0.0112(40)_{\text{SU}(2)}(14)_{\text{EM}}. \quad (5.12)$$

The first error comes from that in Eq. (5.6), while the second from that in Eq. (5.11). The joint quantity $\delta R_{K\pi}$ is of particular importance, as it has been shown that it can be computed from first-principles non-perturbatively on the lattice. The estimation in Eq. (5.12) is compatible with the most recent lattice determinations of this quantity

$$\delta R_{K\pi} = -0.0126(14) \quad [6], \quad (5.13)$$

$$\delta R_{K\pi} = -0.0086(41) \quad [7], \quad (5.14)$$

but with a more conservative uncertainty. Despite this fact, as we will see our final result is currently completely dominated by the uncertainty in Eq. (4.16).

Using the experimental value [5]

$$\frac{\Gamma(K \rightarrow l\bar{\nu}_l[\gamma])}{\Gamma(\pi \rightarrow l\bar{\nu}_l[\gamma])} = 1.3367(32)_{\text{exp}}, \quad (5.15)$$

together with the QED correction in Eq. (5.11) and the values for m_{K^\pm} , m_{π^\pm} , m_μ reported in [5], following Eq. (1.1) we arrive at

$$\frac{f_{K^\pm}|V_{us}|}{f_{\pi^\pm}|V_{ud}|} = 0.27604(33)_{\text{exp}}(19)_{\text{EM}}. \quad (5.16)$$

Finally, from our result in Eq. (5.7), we obtain

$$\frac{|V_{us}|}{|V_{ud}|} = 0.2330(11)_{\text{stat}}(17)_{\chi-\text{cont}}(5)_{\text{SU}(2)}(2)_{\text{EM}}(3)_{\text{exp}}. \quad (5.17)$$

Employing the value of $|V_{ud}|$ from super-allowed β -decays $|V_{ud}| = 0.97367(32)_{\beta-\text{dec.}}$ [5] and neglecting $|V_{ub}|$, whose value squared is $O(10^{-5})$ [5] and thus negligible to the current precision, we obtain

$$|V_{us}| = 0.2269(13)_{\text{stat}}(15)_{\chi-\text{cont}}(4)_{\text{SU}(2)}(2)_{\text{EM}}(2)_{\beta-\text{dec.}}(2)_{\text{exp}}, \quad (5.18)$$

$$|V_{ud}|^2 + |V_{us}|^2 = 0.9995(6)_{\text{stat}}(7)_{\chi-\text{cont}}(2)_{\text{SU}(2)}(1)_{\text{EM}}(7)_{\beta-\text{dec.}}(1)_{\text{exp}}. \quad (5.19)$$

For completeness, we also test employing the $N_f = 2+1+1$ lattice result $|V_{us}| = 0.22328(58)_{|V_{us}|}$ determined from $f_+(0)$ [8] together with our result in Eq. (5.17) to determine $|V_{ud}|$, from which we obtain

$$|V_{ud}|^2 + |V_{us}|^2 = 0.9682(87)_{\text{stat}}(134)_{\chi-\text{cont}}(39)_{\text{SU}(2)}(16)_{\text{EM}}(50)_{|V_{us}|}(24)_{\text{exp}}, \quad (5.20)$$

which is at 1.8σ from the Standard Model unitarity constraint.

If we repeat the same exercise but using the $N_f = 2+1$ lattice result $|V_{us}| = 0.22377(75)_{|V_{us}|}$ [8] we find

$$|V_{ud}|^2 + |V_{us}|^2 = 0.9724(87)_{\text{stat}}(180)_{\chi-\text{cont}}(39)_{\text{SU}(2)}(16)_{\text{EM}}(65)_{|V_{us}|}(24)_{\text{exp}}, \quad (5.21)$$

which is at 1.5σ from unitarity.

We see that our final uncertainty is completely dominated by that of the lattice determination of f_K/f_π in Eq. (4.16), in spite of the conservative choices we took for the uncertainties related to the strong isospin-breaking and QED effects.

6 Conclusions

In this work we have presented results for f_K/f_π in pure isoQCD, in addition to $|V_{us}|/|V_{ud}|$, where strong isospin-breaking and QED effects have been included, which allows to perform a test of the unitarity of the first row of the CKM matrix. Two important features of our construction are that (i) it is based on a combination of a Wilson unitary action and a mixed action with Wilson twisted mass valence fermions [1, 2], and (ii) that it is based on f_π to set the scale. This latter point allows

to avoid any systematic uncertainty related to the continuum-limit extrapolation of theory scales like t_0 or w_0 . We quote as our main results

$$\frac{f_K}{f_\pi} = 1.1872(59)_{\text{stat}}(84)_{\chi-\text{cont}}[103], \quad (6.1)$$

$$\frac{f_{K^\pm}}{f_{\pi^\pm}} = 1.1848(59)_{\text{stat}}(84)_{\chi-\text{cont}}(24)_{\text{SU}(2)}[105], \quad (6.2)$$

$$\frac{|V_{us}|}{|V_{ud}|} = 0.2330(11)_{\text{stat}}(17)_{\chi-\text{cont}}(5)_{\text{SU}(2)}(2)_{\text{EM}}(3)_{\text{exp}}[21], \quad (6.3)$$

the first of which is an unambiguous prediction of $N_f = 2 + 1$ pure isoQCD and can be directly compared to other groups, once the input in Eq. (1.2) has been fixed.

Despite the conservative error choices for the strong isospin-breaking effects and QED corrections, we observe that the uncertainty in these results is still completely dominated by the lattice determination of f_K/f_π . Increased statistics in the ensembles that contribute more to the statistical error in Fig. 4 is expected to help in reducing the error in our results. With respect to the systematic uncertainty coming from the model variation in the chiral-continuum extrapolations, it is important to note that we have included ensembles as fine as $a \approx 0.039$ fm and one (E250, $a \approx 0.063$ fm) at the physical pion mass $m_\pi \approx 130$ MeV. As pointed out in Section 4, we find the systematic uncertainty to be dominated by the chiral dependence of f_K/f_π . Thus, further ensembles at the physical point for finer lattice spacings, in addition to increased statistics in E250, are expected to substantially help in constraining the chiral-continuum extrapolation. The inclusion of NNLO χ PT terms are also relevant in this respect, for which the inclusion of other chiral trajectories than the $\text{tr}(M_q) \approx \text{const.}$ one employed here could be of substantial help.

Acknowledgments

The authors want to thank Alberto Ramos for the very useful discussions and critical reading of a previous version of the manuscript. We also want to thank Gregorio Herdoiza and Carlos Pena for help in the data generation, fruitful discussions and feedback on a previous version of the manuscript. We are grateful to our colleagues in the CLS initiative for sharing ensembles. We acknowledge PRACE for awarding us access to MareNostrum at Barcelona Supercomputing Center (BSC), Spain and to HAWK at GCS@HLRS, Germany. The authors thankfully acknowledge the computer resources at MareNostrum and the technical support provided by Barcelona Supercomputing Center (FI-2020-3-0026). We thank CESGA for granting access to Finis Terrae II. We also acknowledge support from the Spanish Research Agency (Agencia Estatal de Investigación) through national project CNS2022-13600, AEI/MCIU through grant PID2023-148162NB-C21 and ASFAE/2022/020.

A Appendix: QCD scheme variation and impact

In this Appendix we test the impact of modifying the definition of isoQCD by taking different values of $m_{\pi,K}^{\text{ph}}$ and f_π^{ph} with respect to those in Eq. (1.2). In particular, we take the values given in [40]

$$m_\pi^{\text{ph}} = 134.8(3) \text{ MeV}, \quad m_K^{\text{ph}} = 494.2(3) \text{ MeV}, \quad f_\pi^{\text{ph}} = 130.4(2) \text{ MeV}. \quad (\text{A.1})$$

Repeating the analysis in Section 4 with this new input, we see no change in the result in Eq. (4.16) to the precision obtained. This is expected since the two schemes are very similar in terms of the numerical values of the input quantities.

For completeness, we also quote the result for the derivatives of f_K/f_π with respect to the input quantities in Table 4. These derivatives are estimated using the automatic differentiation tools implemented in the `ADerrors` package [16].

$\frac{\partial(f_K/f_\pi)}{\partial m_\pi^{\text{ph}}} \frac{m_\pi^{\text{ph}}}{f_K/f_\pi} \Big _{\text{Edinburgh}}$	$\frac{\partial(f_K/f_\pi)}{\partial m_K^{\text{ph}}} \frac{m_K^{\text{ph}}}{f_K/f_\pi} \Big _{\text{Edinburgh}}$	$\frac{\partial(f_K/f_\pi)}{\partial f_\pi^{\text{ph}}} \frac{f_\pi^{\text{ph}}}{f_K/f_\pi} \Big _{\text{Edinburgh}}$
-0.0208	0.4032	-0.3824

Table 4: Derivatives of f_K/f_π with respect to the input quantities $m_{\pi,K}^{\text{ph}}$, f_π^{ph} used to define the physical point, which can be used to convert our results for f_K/f_π in Eq. (4.16) to any other scheme defined by different values of $m_{\pi,K}^{\text{ph}}$, f_π^{ph} in isoQCD. The derivatives are evaluated at the isoQCD values given by the Edinburgh Consensus in Eq. (1.2).

References

- [1] (ALPHA), A. Bussone, A. Conigli, J. Frison, G. Herdoíza, C. Pena, D. Preti et al., *Hadronic physics from a Wilson fermion mixed-action approach: Setup and scale setting*, [2510.20450](#).
- [2] (ALPHA), A. Bussone, A. Conigli, J. Frison, G. Herdoíza, C. Pena, D. Preti et al., *Hadronic physics from a Wilson fermion mixed-action approach: charm quark mass and $D_{(s)}$ meson decay constants*, *Eur. Phys. J. C* **84** (2024) 506, [\[2309.14154\]](#).
- [3] W. J. Marciano and A. Sirlin, *Radiative corrections to pi(lepton 2) decays*, *Phys. Rev. Lett.* **71** (1993) 3629–3632.
- [4] V. Cirigliano and H. Neufeld, *A note on isospin violation in Pl2(gamma) decays*, *Phys. Lett. B* **700** (2011) 7–10, [\[1102.0563\]](#).
- [5] (PARTICLE DATA GROUP), S. Navas et al., *Review of particle physics*, *Phys. Rev. D* **110** (2024) 030001.
- [6] M. Di Carlo, D. Giusti, V. Lubicz, G. Martinelli, C. T. Sachrajda, F. Sanfilippo et al., *Light-meson leptonic decay rates in lattice QCD+QED*, *Phys. Rev. D* **100** (2019) 034514, [\[1904.08731\]](#).
- [7] P. Boyle et al., *Isospin-breaking corrections to light-meson leptonic decays from lattice simulations at physical quark masses*, *JHEP* **02** (2023) 242, [\[2211.12865\]](#).
- [8] (FLAVOUR LATTICE AVERAGING GROUP (FLAG)), Y. Aoki et al., *FLAG Review 2024*, [2411.04268](#).
- [9] M. Bruno et al., *Simulation of QCD with $N_f = 2 + 1$ flavors of non-perturbatively improved Wilson fermions*, *JHEP* **02** (2015) 043, [\[1411.3982\]](#).

- [10] D. Mohler, S. Schaefer and J. Simeth, *CLS 2+1 flavor simulations at physical light- and strange-quark masses*, *EPJ Web Conf.* **175** (2018) 02010, [[1712.04884](#)].
- [11] (ALPHA), R. Frezzotti, P. A. Grassi, S. Sint and P. Weisz, *Lattice QCD with a chirally twisted mass term*, *JHEP* **08** (2001) 058, [[hep-lat/0101001](#)].
- [12] C. Pena, S. Sint and A. Vladikas, *Twisted mass QCD and lattice approaches to the Delta I = 1/2 rule*, *JHEP* **09** (2004) 069, [[hep-lat/0405028](#)].
- [13] M. Lüscher, *Properties and uses of the Wilson flow in lattice QCD*, *JHEP* **08** (2010) 071, [[1006.4518](#)]. [Erratum: *JHEP* 03, 092 (2014)].
- [14] (BMW), S. Borsányi, S. Dürr, Z. Fodor, C. Hoelbling, S. D. Katz, S. Krieg et al., *High-precision scale setting in lattice QCD*, *JHEP* **09** (2012) 010, [[1203.4469](#)].
- [15] (ALPHA), U. Wolff, *Monte Carlo errors with less errors*, *Comput. Phys. Commun.* **156** (2004) 143–153, [[hep-lat/0306017](#)]. [Erratum: *Comput.Phys.Commun.* 176, 383 (2007)].
- [16] A. Ramos, *Automatic differentiation for error analysis of Monte Carlo data*, *Comput. Phys. Commun.* **238** (2019) 19–35, [[1809.01289](#)].
- [17] M. Bruno, T. Korzec and S. Schaefer, *Setting the scale for the CLS 2 + 1 flavor ensembles*, *Phys. Rev. D* **95** (2017) 074504, [[1608.08900](#)].
- [18] S. Kuberski, *Low-mode deflation for twisted-mass and RHMC reweighting in lattice QCD*, *Comput. Phys. Commun.* **300** (2024) 109173, [[2306.02385](#)].
- [19] E. T. Neil and J. W. Sitzer, *Model averaging approaches to data subset selection*, *Phys. Rev. E* **108** (2023) 045308, [[2305.19417](#)].
- [20] M. Luscher and S. Schaefer, *Lattice QCD with open boundary conditions and twisted-mass reweighting*, *Comput. Phys. Commun.* **184** (2013) 519–528, [[1206.2809](#)].
- [21] A. D. Kennedy, I. Horvath and S. Sint, *A New exact method for dynamical fermion computations with nonlocal actions*, *Nucl. Phys. B Proc. Suppl.* **73** (1999) 834–836, [[hep-lat/9809092](#)].
- [22] M. A. Clark and A. D. Kennedy, *The RHMC algorithm for two flavors of dynamical staggered fermions*, *Nucl. Phys. B Proc. Suppl.* **129** (2004) 850–852, [[hep-lat/0309084](#)].
- [23] M. A. Clark and A. D. Kennedy, *Accelerating dynamical fermion computations using the rational hybrid Monte Carlo (RHMC) algorithm with multiple pseudofermion fields*, *Phys. Rev. Lett.* **98** (2007) 051601, [[hep-lat/0608015](#)].
- [24] M. Lüscher, “Charm and strange quark in openqcd simulations.” <http://luscher.web.cern.ch/luscher/openQCD/>, 2019.
- [25] G. Colangelo, A. Fuhrer and C. Haefeli, *The pion and proton mass in finite volume*, *Nucl. Phys. B Proc. Suppl.* **153** (2006) 41–48, [[hep-lat/0512002](#)].
- [26] G. Colangelo, S. Durr and C. Haefeli, *Finite volume effects for meson masses and decay constants*, *Nucl. Phys. B* **721** (2005) 136–174, [[hep-lat/0503014](#)].

[27] N. Husung, *Logarithmic corrections to $O(a)$ and $O(a^2)$ effects in lattice QCD with Wilson or Ginsparg–Wilson quarks*, *Eur. Phys. J. C* **83** (2023) 142, [[2206.03536](#)]. [Erratum: *Eur. Phys. J. C* 83, 144 (2023)].

[28] J. Frison, *Towards fully bayesian analyses in Lattice QCD*, [2302.06550](#).

[29] M. Bruno and R. Sommer, *On fits to correlated and auto-correlated data*, *Comput. Phys. Commun.* **285** (2023) 108643, [[2209.14188](#)].

[30] V. Cirigliano and I. Rosell, *$\pi/K \rightarrow e$ anti- $\nu(e)$ branching ratios to $O(e^{**2} p^{**4})$ in Chiral Perturbation Theory*, *JHEP* **10** (2007) 005, [[0707.4464](#)].

[31] (CLQCD), Z.-C. Hu et al., *Quark masses and low-energy constants in the continuum from the tadpole-improved clover ensembles*, *Phys. Rev. D* **109** (2024) 054507, [[2310.00814](#)].

[32] (QCDSF–UKQCD), V. G. Bornyakov, R. Horsley, Y. Nakamura, H. Perlt, D. Pleiter, P. E. L. Rakow et al., *Flavour breaking effects in the pseudoscalar meson decay constants*, *Phys. Lett. B* **767** (2017) 366–373, [[1612.04798](#)].

[33] S. Dürr et al., *Leptonic decay-constant ratio f_K/f_π from lattice QCD using 2+1 clover-improved fermion flavors with 2-HEX smearing*, *Phys. Rev. D* **95** (2017) 054513, [[1601.05998](#)].

[34] (RBC, UKQCD), T. Blum et al., *Domain wall QCD with physical quark masses*, *Phys. Rev. D* **93** (2016) 074505, [[1411.7017](#)].

[35] (MILC), A. Bazavov et al., *Results for light pseudoscalar mesons*, *PoS LATTICE2010* (2010) 074, [[1012.0868](#)].

[36] (BMW), S. Durr, Z. Fodor, C. Hoelbling, S. D. Katz, S. Krieg, T. Kurth et al., *The ratio FK/Fpi in QCD*, *Phys. Rev. D* **81** (2010) 054507, [[1001.4692](#)].

[37] (HPQCD, UKQCD), E. Follana, C. T. H. Davies, G. P. Lepage and J. Shigemitsu, *High Precision determination of the π , K , D and $D(s)$ decay constants from lattice QCD*, *Phys. Rev. Lett.* **100** (2008) 062002, [[0706.1726](#)].

[38] S. Descotes-Genon and B. Moussallam, *Radiative corrections in weak semi-leptonic processes at low energy: A Two-step matching determination*, *Eur. Phys. J. C* **42** (2005) 403–417, [[hep-ph/0505077](#)].

[39] B. Ananthanarayan and B. Moussallam, *Four-point correlator constraints on electromagnetic chiral parameters and resonance effective Lagrangians*, *JHEP* **06** (2004) 047, [[hep-ph/0405206](#)].

[40] S. Aoki et al., *Review of lattice results concerning low-energy particle physics*, *Eur. Phys. J. C* **77** (2017) 112, [[1607.00299](#)].